pH-Responsive Freeze-Thawed Polyvinyl Alcohol/Chitosan Hydrogels for Topical Delivery of Anti-Inflammatory, Antioxidant, and Antibacterial *Piper betle* Leaf Extract Toward Wound Healing Applications

Nga Hoang Nguyen Do[1,2], Ha Vu Le[1,2], Khoa Dang Nguyen[1,2], and Anh Cam Ha[1,2*]

[1]*Faculty of Chemical Engineering, Ho Chi Minh City University of Technology (HCMUT), 268 Ly Thuong Kiet Street, Dien Hong Ward, Ho Chi Minh City 740500, Vietnam*

[2]*Vietnam National University Ho Chi Minh City, Linh Xuan Ward, Ho Chi Minh City 721400, Vietnam*

* ***Corresponding author:***

email: hcanh@hcmut.edu.vn

Received: November 16, 2025
Accepted: April 29, 2026

DOI: 10.22146/ijc.113151

Abstract: Piper betle *leaf extract (BLE) shows strong anti-inflammatory, antioxidant, and antibacterial activities. However, its application is limited due to poor water solubility, oxidative instability, and rapid clearance from the application site. To address these challenges, a crosslinker-free polyvinyl alcohol/chitosan (PVA/CS) hydrogel encapsulating BLE was developed via repeated freeze-thaw cycles. The hydrogel exhibited an interconnected porous structure, enabling stable incorporation of BLE without phase separation. As a result, the PVA/CS/BLE hydrogel achieved a high gel fraction of 89.6–94.0%, a substantial swelling capacity of 208–220%, and favorable mechanical properties, including a tensile modulus of 122.00 kPa, a tensile strength of 672.00 kPa, and an elongation at break of 242.89%. Notably, BLE release was pH-responsive, with accelerated release under simulated acute wound conditions (pH 6.5), allowing for an initial burst release of BLE to combat early-stage infections and inflammation, followed by sustained release to support wound healing. Overall, these features indicate that the PVA/CS/BLE hydrogel patch exhibits tunable structure, robust mechanical properties, and pH-responsive release behavior, highlighting its potential as a platform for delivering BLE topically in wound-healing applications.*

Keywords: *hybrid hydrogel; freeze-thaw; Betel leaf extract; characterization; controlled release*

■ INTRODUCTION

Hybrid hydrogels made from polyvinyl alcohol (PVA) and chitosan (CS) have emerged as a promising type of polymeric matrix for biomedical delivery systems due to their exceptional combination of physical, chemical, and biological properties. Compared to conventional hydrogels, the PVA/CS system demonstrates superior mechanical strength, thanks to the physically crosslinked PVA crystallites, and enhanced bioactivity due to CS's cationic nature [1]. This dual-network structure not only ensures structural integrity but also provides intrinsic antimicrobial, hemostatic, and wound-healing properties - features that are often lacking or require additional additives in single-component or synthetic hydrogels [2-3]. Additionally, CS contributes to the pH-responsive behavior of the matrix, allowing for the selective and accelerated release of therapeutic agents in the acidic environment of inflamed or infected wounds [4]. Unlike chemically crosslinked hydrogels, which may raise concerns about cytotoxicity, PVA/CS hydrogels are formed through multiple freeze-thaw cycles, eliminating the need for toxic crosslinkers and making them inherently safer and more biocompatible [5]. Their high-water retention, adjustable porosity, and capacity to encapsulate a wide range of bioactive compounds, including plant-derived substitutes, position PVA/CS hydrogels as an advanced and versatile platform for smart wound dressings and controlled drug delivery [2,6-7].

PVA/CS hybrid hydrogels have emerged as effective

carriers for natural compounds in wound healing applications, addressing various limitations associated with the direct use of phytochemicals. These hydrogels combine the mechanical strength, film-forming capacity, and water-retention ability of PVA with the biocompatibility, intrinsic antibacterial properties, and mucoadhesiveness of CS [8]. This results in a physically crosslinked, pH-responsive matrix that is suitable for topical biomedical use. Natural bioactive compounds, while rich in antioxidant, anti-inflammatory, and antimicrobial properties, often face challenges such as poor aqueous solubility, limited stability, and uncontrolled diffusion at the site of application [9-10]. The PVA/CS hydrogel platform addresses these issues by forming a three-dimensional polymeric network that encapsulates active compounds, protects them from degradation, and allows for sustained, localized release directly into the wound bed [11]. Recent studies have confirmed the effectiveness of PVA/CS hydrogels in delivering plant-derived compounds such as *Calophyllum inophyllum* extract, traditional Tibetan herbal formulations, epigallocatechin gallate, gallic acid, and tea tree oil for the treatment of chronic ulcers, diabetic wounds, and infected lesions [12-16]. The controlled-release behavior of these systems extends therapeutic effects, reduces dosing frequency, and ensures consistent bioavailability, significant advantages over traditional formulations or direct applications. Moreover, the ability of hydrogels to maintain a moist environment, adapt to irregular wound surfaces, and promote cell proliferation makes them especially valuable for managing complex wounds [11]. As a result, incorporating natural compounds into PVA/CS hydrogels is a promising, increasingly popular strategy in regenerative medicine and phytopharmaceutical delivery.

Betel leaf extract (BLE, *Piper betle*) is derived from a widely used ethnomedicinal plant found in Southeast Asia. This extract is rich in phytochemicals, including flavonoids, polyphenols, alkaloids, tannins, and essential oils such as eugenol, chavibetol, and hydroxychavicol [17]. These components provide a range of bioactivities, including strong antioxidant, anti-inflammatory, antibacterial, and wound-healing properties, making it a promising natural treatment for topical wound care [11]. However, the topical application of BLE is limited by several intrinsic challenges, including high volatility, low water solubility, oxidative instability, and rapid clearance from the application site [18-19]. To address these challenges, recent research has focused on hydrogel-based encapsulation techniques to protect BLE from degradation, facilitate sustained release, and enhance its targeted effectiveness in wound healing applications. Several studies have developed PVA/CS-based hydrogels incorporating BLE in the form of thermosensitive injectable gels, wound plaster, and thin films with favorable wound-healing properties [11,20-21]. However, these systems are typically fabricated using simple casting, thermogelation, or chemically crosslinked networks, which often require additional crosslinking agents that may introduce potential cytotoxicity and limit long-term biocompatibility. Unlike chemical crosslinking approaches, freeze-thaw cycling offers a superior, crosslinker-free alternative. This physical gelation strategy induces the formation of PVA crystallite domains and promotes chain entanglement with CS, producing a stable three-dimensional network without toxic additives. The freeze-thaw process generates interconnected porous structures with enhanced mechanical integrity and structural stability, while repeated freeze-thaw cycles further increase network density and enable tunable and sustained release behavior.

In this context, we present the first crosslinker-free PVA/CS hydrogel incorporating BLE fabricated via freeze-thaw cycling. The hydrogel was developed as a structurally tunable platform for topical wound treatment. The effects of polymer composition, number of freeze-thaw cycles, and BLE loading on the hydrogel architecture were systematically investigated. Comprehensive characterization was also performed, including swelling behavior, gel fraction, and tensile properties, together with evaluation of BLE release kinetics under simulated physiological (pH 7.4) and acute wound (pH 6.5) environments. The results demonstrated that this physically crosslinked, crosslinker-free hydrogel allows controlled, pH-

responsive delivery of BLE while maintaining robust mechanical performance, advancing the potential of PVA/CS hydrogels in wound care applications.

■ EXPERIMENTAL SECTION

Materials

CS (molecular weight 158 kDa, degree of deacetylation 96.5%) was supplied by Vietnam Food Company. PVA (molecular weight 85–124 kDa, degree of hydrolysis 99%) was purchased from Sigma-Aldrich. Fresh betel leaves (*P. betle* L.) were collected from Hoc Mon Province, Vietnam, in 2023, washed thoroughly with distilled water to remove impurities, and air-dried in the shade to a moisture content below 12%. Acetic acid (CH_3COOH), Tween 80, ethanol (C_2H_5OH), monosodium phosphate dihydrate ($NaH_2PO_4{\cdot}2H_2O$), sodium biphosphate dodecahydrate ($Na_2HPO_4{\cdot}12H_2O$), sodium hydroxide (NaOH), sodium nitrite ($NaNO_2$), and aluminum chloride hexahydrate ($AlCl_3{\cdot}6H_2O$) were obtained from commercial suppliers in analytical grade. In the quantification of total flavonoid content, rutin ($C_{27}H_{30}O_{16}$, 88.5% purity) was used as a reference standard, following the United States Pharmacopeia specification (catalog no. 1606503), and was obtained from China. L-ascorbic acid (99.7% purity, Xilong, China), methanol (CH_3OH, Xilong, China), and 1,1-diphenyl-2-picrylhydrazyl (DPPH, 97% purity, TCi, Japan) were used in the antioxidant activity assay. Hyaluronidase (HYAL, 400–1000 U/mg), hyaluronic acid (HA, 98% purity, Sigma-Aldrich), bovine serum albumin (BSA, 98% purity, China), and ursolic acid (98% purity, Macklin, China) as a positive control were employed in the anti-inflammatory activity assay. Mueller-Hinton agar (MHA, Himedia, India), dimethyl sulfoxide (DMSO, 99.5% purity, Xilong, China) as a negative control and as a solvent for sample dissolution, and amikacin (Sigma-Aldrich, USA) as a positive control were used in the antibacterial assay

Bioactive assays BLE

The *in vitro* anti-inflammatory activity of BLE was assessed using a hyaluronidase (HYAL) inhibition assay [22]. Initially, 25 µL of the BLE solution, 100 µL of the HYAL solution (4 U/mL, pH 5.4), and 100 µL of phosphate buffer (pH 7.0) were incubated at 37 °C for 10 min. Next, 100 µL of HA (0.03% in 300 mM sodium phosphate, pH 5.4) was added to the mixture, followed by incubation at 37 °C for an additional 45 min. Subsequently, 1 mL of 0.1% BSA solution was added, and the mixture was incubated at room temperature for another 10 min. The turbidity of the reaction mixture was then measured at 600 nm to quantify HYAL inhibition. The IC_{50} value, defined as the concentration of BLE required to inhibit 50% of the enzyme activity, was calculated from the dose-response curve of inhibition percentage versus BLE concentration. Ursolic acid was used as the positive control.

The antioxidant activity of BLE was evaluated based on its ability to scavenge DPPH free radicals. The EC_{50} value of BLE and ascorbic acid, as the positive control, was defined as the concentration required to neutralize 50% of DPPH radicals. BLE and ascorbic acid solutions with various concentrations were prepared in 80% methanol, while a 0.1 mM DPPH solution was also prepared in the same solvent. Reaction mixtures were prepared as follows: (1) 1.8 mL of BLE solution with 3.2 mL of DPPH solution; (2) 1.8 mL of BLE solution with 3.2 mL of 80% methanol; (3) 1.8 mL of 80% methanol with 3.2 mL of DPPH solution. The DPPH radical scavenging efficiency (E%) was calculated according to Eq. (1);

$$E\ (\%) = \frac{A_{(1)} - \left(A_{(2)} - A_{(3)}\right)}{A_{(1)}} \times 100\% \quad (1)$$

where $A_{(1)}$, $A_{(2)}$, and $A_{(3)}$ represent the absorbance values of the corresponding mixtures measured at 517 nm.

The antibacterial activity of BLE was assessed against *Staphylococcus aureus* ATCC 29213 using the agar well diffusion method. Bacterial suspensions were spread on MHA plates at a density of 10^4 CFU/mL. Wells with an 8 mm diameter were filled with 60 µL of BLE solution (200 mg/mL in DMSO). The plates were incubated at 35–37 °C for 16–24 h, and the inhibition zones were measured to evaluate antibacterial activity. For the minimum inhibitory concentration (MIC) test, BLE was serially diluted to concentrations of 10.00, 5.00, 2.50, 1.25, 0.625, 0.32, and 0.16 mg/mL in the same medium. The procedure followed for the MIC test was

identical to that for the diffusion assay, and the MIC was determined as the concentration that completely inhibited visible bacterial growth.

Characterization of PVA/CS/BLE hydrogels

Hydrogel patches were lyophilized using Toption TPV-50F freeze-dryer to produce a monolithic form for studying their morphologies. The dried hydrogels were coated with a Cr layer under an Ar environment before analysis by field emission scanning electron microscope (FE-SEM, TESCAN, MIRA LMU, Czech Republic). Fourier transform infrared spectroscopy (FTIR, Alpha II, Bruker, Germany) was employed to analyze the chemical structure of CS, PVA, BLE, and hydrogels with and without the extract. Their FTIR spectra were plotted in the wavenumber range of 500–4000 cm^{-1} at a resolution of 4 cm^{-1}.

The swelling capacity of the hydrogels was assessed by comparing their weights before and after immersion in phosphate buffer (pH 7.4) at room temperature. Briefly, the hydrogels were first dried at 40 °C for 24 h to remove residual moisture and achieve a constant weight, then cut into pieces of 2 × 2 cm^2, and weighed to determine the initial mass (m_0, g). Then, the hydrogels (n = 3) were soaked in the buffer, and after specific times (3, 6, 9, and 12 h), the samples were lifted out, strained through a sieve, and weighed again (m_t, g). The swelling ratio of each hydrogel was calculated from Eq. (2) as follows.

$$\text{Swelling ratio } (\%) = \frac{m_t - m_0}{m_0} \times 100\% \quad (2)$$

To measure the gel fraction, the hydrogel patches were first dried at 40 °C for 24 h, cut into 2 × 2 cm^2 pieces, and weighed to determine the initial dry mass (m_0, g). The samples were subsequently placed in a phosphate buffer solution (pH 7.4) at room temperature. After 12 h of incubation, the samples were removed from the buffer, rinsed gently with distilled water, and dried in an oven at 50 °C until reaching a constant weight (m_f, g). The gel fraction, representing the degree of crosslinking within the hydrogel network, was calculated using Eq. (3). Each experiment was performed in triplicate (n = 3), and the average value with standard deviation was reported.

$$\text{Gel fraction } (\%) = \frac{m_f}{m_0} \times 100\% \quad (3)$$

The tensile behavior of the hydrogels was examined using a universal testing machine (Zwick/Roell Z010) in compliance with ISO 527-3. Rectangular specimens (20 × 150 mm) were prepared and tested under tension using a 0.12 N load cell at a crosshead speed of 50 mm/min. The resulting stress-strain profiles were used to calculate the elastic modulus, tensile strength, and elongation at break of the hydrogels.

In vitro *release study of PVA/CS/BLE hybrid hydrogels*

BLE release from the hybrid hydrogels was evaluated using samples with different BLE loadings. The prepared hydrogels were cut into 2 × 2 cm^2 pieces, each weighing approximately 0.5 g. Each sample was then immersed in 5 mL of phosphate buffer solution (pH 6.5 or 7.4) at 37 °C. At predetermined time intervals, 1 mL of the release medium was withdrawn to determine the amount of BLE released using UV-vis spectroscopy at 280 nm and immediately replaced with an equal volume of fresh buffer to maintain a constant volume. The cumulative BLE release (CDR) was calculated according to Eq. (4). All experiments were performed in triplicate (n = 3). BLE calibration curves in both pH 6.5 and 7.4 buffers were established by measuring standard BLE solutions at concentrations of 10, 20, 30, 40, 50, 60, 70, 80, 90, and 100 μg/mL (Fig. S1);

$$\text{CDR } (\%) = \frac{Q_t}{Q_0} \times 100\% \quad (4)$$

where Q_t and Q_0 are, respectively, the amounts of BLE in the medium at each sampling time and in the hydrogel before release.

The experimental release data were analyzed using the Weibull model (Eq. (5)) to compare the release behavior of different PVA/CS/BLE formulations and to evaluate the influence of pH on their release characteristics;

$$\frac{M_t}{M_\infty} = 1 - e^{-\left(\frac{t}{A}\right)^B} \quad (5)$$

where $\frac{M_t}{M_\infty}$ is a fraction of the released at a determined time (t). (A) and (B) are model coefficients.

Preparation of PVA/CS hydrogels loading betel leaf extract by freeze-thaw method

BLE was obtained following the procedure described in our previous work [19]. Briefly, 30 g of pulverized betel leaf powder was mixed with 80% ethanol at a solid-to-liquid ratio of 1:10 g/mL and subjected to ultrasonic-assisted extraction for 20 min. The mixture was then filtered, and the filtrate was concentrated by vacuum evaporation to obtain crude BLE. For hydrogel preparation, 1.6 g of BLE was dispersed in 100 mL of distilled water containing 2.0 v/v% Tween 80, and the mixture was sonicated for 5 min to obtain a homogeneous BLE solution. A 12 w/v% PVA solution was prepared by dissolving 12 g of PVA flakes in 100 mL of distilled water at 80 °C, and a 2 w/v% CS solution was prepared by dissolving 2 g of CS in 100 mL of 1 v/v% acetic acid. The PVA and CS solutions were mixed at a 4:1 volume ratio at room temperature to form the PVA/CS blend. The BLE solution was then added dropwise to the PVA/CS mixture blend under magnetic stirring at 750 rpm for 1 h. Distilled water was added to adjust to the desired final volume, yielding homogeneous PVA/CS/BLE hydrogel blends containing BLE at concentrations of 2000, 3000, and 4000 µg/mL. The mixture was sonicated to remove entrapped air bubbles. The resulting mixture was cast into plastic Petri dishes and subjected to 5 freeze-thaw cycles (freezing at −25 °C for 18 h and thawing at room temperature for 6 h per cycle) to obtain the hybrid hydrogels. Blank hydrogels with different polymer contents and freeze-thaw cycles were also synthesized using this procedure (Table S1).

■ RESULTS AND DISCUSSION

Phytochemical Yield and Bioactivities of BLE

Under the selected extraction conditions (80% ethanol, 20 min extraction, solid-to-liquid ratio of 1:10 g/mL, ultrasound-assisted [19]). The obtained BLE exhibited an exceptionally high total flavonoid content (TFC) of 704.85 ± 1.85 mg RE/g dry extract. This value was about six times greater than that achieved using absolute methanol at a 1:7.5 g/mL ratio (111.44 ± 1.36 mg RE/g) [23] and twelve times higher than that obtained with absolute ethanol at the same 1:10 g/mL ratio (56.86 ± 0.14 mg RE/g) [24], emphasizing the superiority of the selected extraction system. The remarkable enhancement in TFC can be attributed to the synergistic effect of ethanol-water polarity balance and acoustic cavitation induced by ultrasound, which improves solubilization and diffusion of both hydrophilic and lipophilic flavonoids [25-26]. Additionally, intrinsic factors such as plant variety and climatic conditions may further account for variations in flavonoid accumulation among different studies. When compared with other plant extracts exhibiting anti-inflammatory activity, the TFC of BLE is considerably higher than that of the ethanolic *Cordia myxa* L. leaf extract (192.24 ± 0.33 mg RE/g) [27], the methanolic *Chrysanthemum procumbens* leaf extract of leaves (230.30 ± 22.11 mg RE/g) [28], and the ethanolic *Viola canescens* wall. Ex Roxb. leaf extract (270.02 ± 1.36 mg RE/g) [29]. Overall, the relatively high TFC of BLE confirms its strong potential as a bioactive extract for supporting the treatment of inflammation-related conditions.

BLE demonstrated multiple biological activities directly relevant to wound-healing and tissue repair, encompassing anti-inflammatory, antioxidant, and antibacterial effects. The anti-inflammatory potential was evaluated through the inhibition of hyaluronidase, an enzyme responsible for degrading hyaluronic acid and enhancing inflammatory responses [30]. BLE showed an IC_{50} value of 46.55 ± 1.70 µg/mL, approximately eight-fold higher than that of ursolic acid, signifying its strong potential to limit enzymatic degradation of hyaluronic acid - a key extracellular matrix component regulating inflammation and hydration during healing. Compared with the reported low inhibition efficiency (13.14–24.23% at 384 µg/mL) of *P. betle* extracts prepared using other solvents [31]. The present BLE demonstrated markedly enhanced activity, reflecting the greater recovery of bioactive compounds under selected extraction conditions.

Oxidative stress plays a pivotal role in inflammation-induced tissue damage [32]. The potent antioxidant performance of BLE, evidenced by a DPPH EC_{50} value of 7.36 ± 0.18 µg/mL, approximately 2.6

times higher than that of ascorbic acid (2.78 ± 0.05 μg/mL), highlights its capacity to neutralize reactive oxygen species (ROS) and suppress redox-mediated inflammatory pathways. This pronounced radical-scavenging capability could be ascribed to its rich phenolic composition, notably eugenol, isoeugenol, hydroxychavicol, chavibetol, allylpyrocatechol, and 4-allyl-1,2-diacetoxybenzene [33], which collectively contribute to ROS quenching, membrane stabilization, and cellular protection.

Furthermore, BLE exhibited antibacterial efficacy, forming a 17 mm inhibition zone against *S. aureus* compared to 23 mm for amikacin as the positive control (Fig. S2), with a MIC value of 1.25 mg/mL (Fig. S3). The antibacterial action was primarily attributed to the synergistic interactions of phenolic and allyl compounds that disrupt bacterial cell walls, impair membrane integrity, and inhibit essential metabolic enzymes, ultimately leading to bacterial death. These combined anti-inflammatory, antioxidant, and antibacterial properties reinforce BLE's therapeutic potential for managing infection-prone or inflamed wounds [34-38]. Accordingly, BLE concentrations in the hydrogel formulations were chosen in the range of 2000–4000 μg/mL, ensuring effective antimicrobial levels above the MIC while maintaining compatibility with the PVA/CS matrix.

Morphological Characteristics of the Hybrid Hydrogels

The morphology of the blank PVA/CS hydrogel was strongly influenced by the polymer composition and freeze-thaw cycles (Figs. S4–S6). Systematic investigations showed that an appropriate balance between CS and PVA was essential to form a continuous and interconnected porous structure. Hydrogels with low CS or PVA contents exhibited weakly crosslinked and irregular morphologies, while those with excessive contents became dense due to excessive crystallite formation and polymer entanglement. Likewise, increasing the number of freeze-thaw cycles enhanced structural cohesion, but excessive cycling led to less-interconnected pores that could hinder swelling and diffusion. Based on these observations, the formulation containing 0.3% CS, 10.0% PVA, and five freeze-thaw cycles was selected as a suitable composition providing a robust yet permeable network for BLE incorporation. The visual images of the prepared PVA/CS and PVA/CS/BLE hydrogels are shown in Fig 1. The blank hydrogel exhibited a translucent white appearance with a smooth surface, whereas the BLE-loaded samples displayed an increasingly yellow coloration proportional to the BLE concentration, confirming the successful incorporation of the extract. The uniform color distribution and absence of phase separation suggest a homogeneous dispersion of BLE within the polymer matrix, indicating good compatibility between the extract and the PVA/CS network.

SEM analysis further elucidated the structural changes of the hydrogels upon BLE loading (Fig 2). The blank hydrogel showed an interconnected porous network typical of physically crosslinked PVA/CS systems formed by freeze-thaw cycling. Upon BLE incorporation, the morphology became more compact, with the initial pores filled by BLE. Increasing BLE concentration from 2000 to 4000 μg/mL slightly disrupted the uniformity of the polymeric structure, likely due to the physical interactions of BLE with PVA

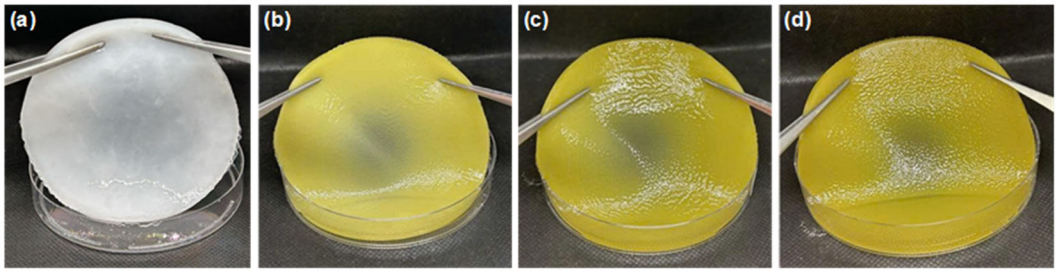

Fig 1. Photographs of (a) blank hydrogel and PVA/CS/BLE hydrogels with different BLE contents of (b) 2000, (c) 3000, and (d) 4000 μg/mL

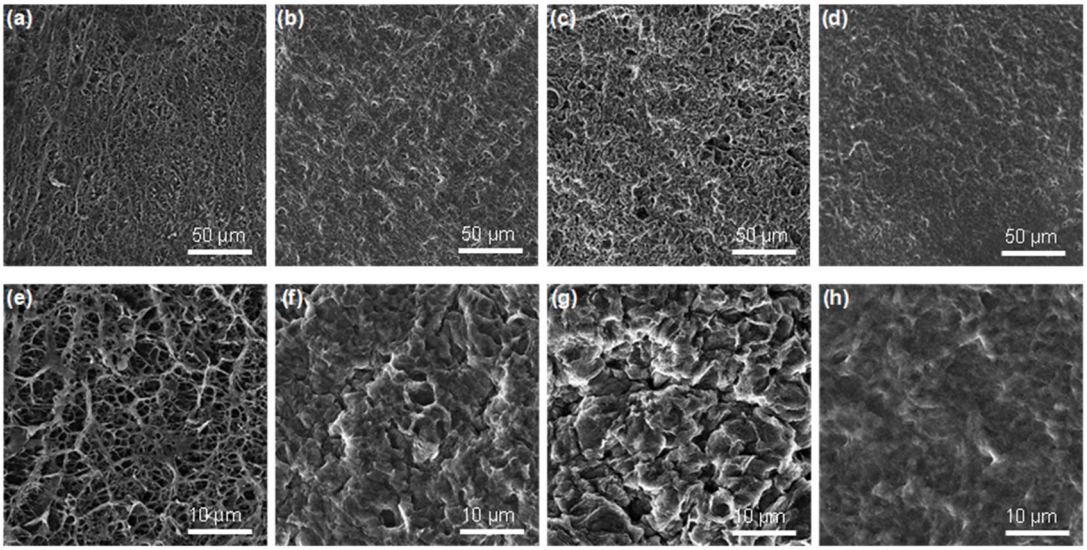

Fig 2. Morphologies of (a,e) PVA/CS hydrogel and PVA/CS/BLE hydrogels with varying BLE content of (b,f) 2000, (c,g) 3000, and (d,h) 4000 µg/mL

and CS, hindering hydrogen-bond formation and crystallite alignment during gelation [39-40].

FTIR Analysis of the BLE-loaded Hybrid Hydrogel

The FTIR spectra of PVA, CS, BLE, and their hybrid hydrogels are shown in Fig 3(a). The PVA spectrum exhibited a broad absorption band around 3300 cm^{-1} corresponding to O–H stretching, a peak near 2940 cm^{-1} associated with C-H stretching, a band at 1420 cm^{-1} assigned to CH_2–OH bending vibrations, and a strong absorption at 1090 cm^{-1} attributed to C–O–C stretching of the PVA backbone [11]. CS displayed characteristic bands at 3430 cm^{-1} (overlapping O–H and N–H stretching), 1646 and 1585 cm^{-1} (C=O stretching and N–H bending of the amide linkage), and 1028–1078 cm^{-1} (C–O–C stretching in the glycosidic bonds) [18,41]. In the PVA/CS hydrogel, the spectrum remained largely dominated by PVA features, as PVA was present at a higher content (10% PVA and 0.3% CS). However, FTIR spectral changes confirmed molecular interactions between the two polymers. The broad O–H/N–H stretching band became wider and shifted slightly toward a lower wavenumber (3280 cm^{-1}), suggesting that the O–H and N–H groups require greater energy for vibrational motion as a result of strengthened intermolecular interactions. This phenomenon was also reported in the CS/PVA hydrogels containing honey and allantoin [39]. Additionally, the characteristic band of CS at 1585 cm^{-1}, corresponding to the N–H bending vibration of the amide linkage, shifted slightly to 1565 cm^{-1} in the PVA/CS hydrogel, indicating the participation of N–H groups in intermolecular hydrogen bonding with PVA's O–H groups [42]. These findings demonstrate that a physically crosslinked PVA/CS network was established through hydrogen-bonding interactions during the freeze-thaw process.

Upon BLE incorporation, the intensities of the characteristic absorption bands at 3270 cm^{-1} (O–H/N–H stretching), 1565 cm^{-1} (N–H bending), and 1090 cm^{-1} (C–O–C stretching) increased, reflecting the additional contribution of BLE functional groups and enhanced hydrogen-bonding interactions among BLE, PVA, and CS. Moreover, the characteristic C–O–C stretching band of BLE at 1040 cm^{-1} and carbonyl band at 1240 cm^{-1} disappeared in the PVA/CS/BLE spectra, likely due to overlap with the strong C–O–C band (1090 cm^{-1}) and restricted vibration of BLE functional groups upon encapsulation. These collective spectral shifts and intensity variations confirm successful immobilization of BLE and the establishment of secondary hydrogen-bonding interactions that stabilize the hybrid hydrogel network, providing a robust foundation for its controlled-release and bioactive performance.

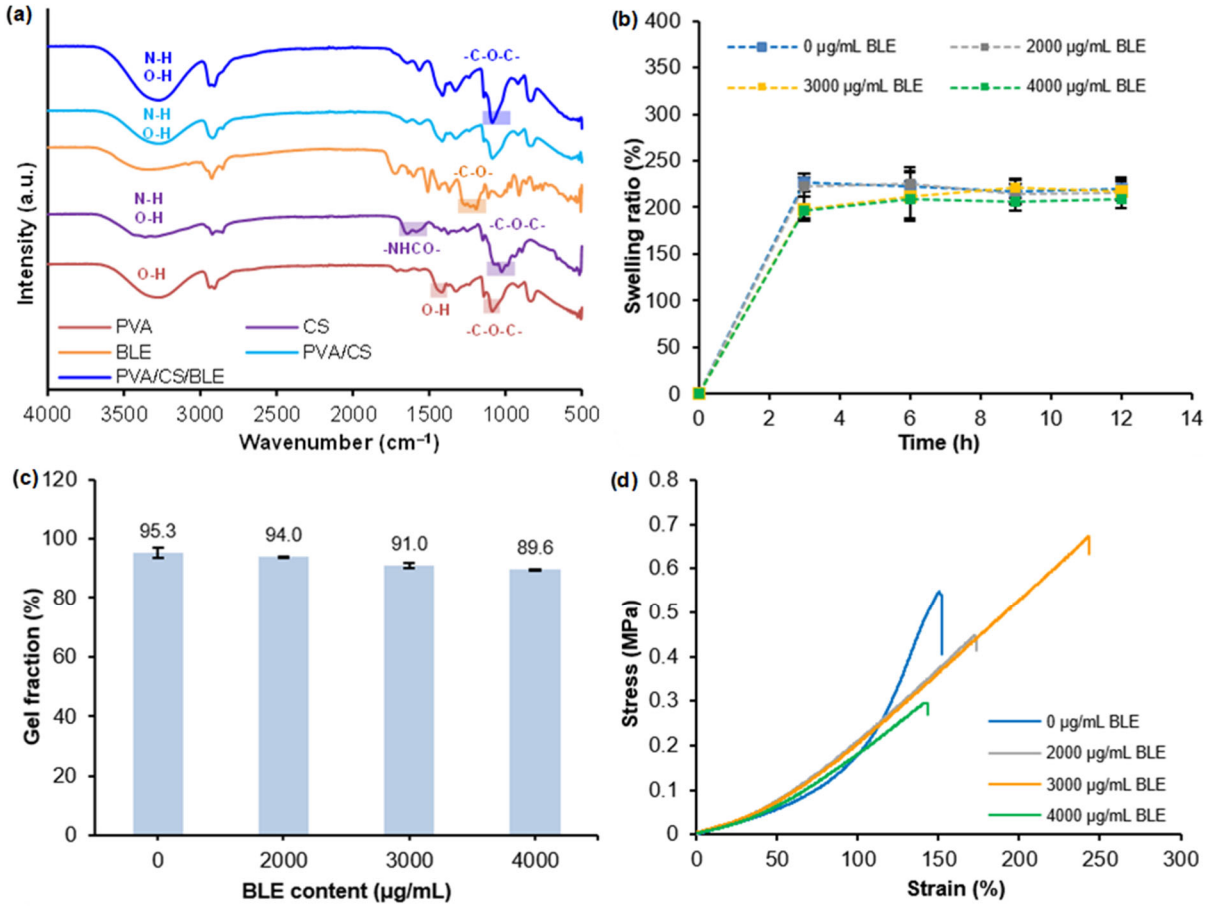

Fig 3. (a) FTIR spectra of components, PVA/CS, and PVA/CS/BLE hydrogels; (b) Effects of BLE content on swelling ratio and (c) gel fraction of hybrid hydrogels; (d) Stress-strain curves of PVA/CS/BLE hydrogels with varying BLE content

Swelling Behavior and Gel Fraction of the Hybrid Hydrogels

The swelling capacity and gel fraction of PVA/CS hydrogels are key indicators of the network's crosslinking density, hydrophilicity, and structural stability, all of which strongly influence the release and mechanical properties of the final material. A systematic investigation (Figs. S7–S8) revealed that both polymer composition and the number of freeze-thaw cycles exerted pronounced effects on these parameters. The swelling ratio increased with CS content from 0.1 to 0.5%, owing to the greater abundance of hydrophilic –OH/–NH_2 groups, which enhanced the network's affinity for water and promoted higher water uptake [8]. However, increasing PVA concentration from 6.0 to 10.0% strengthened hydrogen-bonded crystalline domains, leading to higher PVA crystallinity and denser physical crosslinking. This compact structure restricted water diffusion and reduced the equilibrium swelling ratio, although it simultaneously improved the gel's mechanical integrity and stability [6]. The swelling capacity also decreased with increasing freeze-thaw cycles, as repeated freezing enhanced PVA crystallite formation and densified the polymer network, thereby restricting water penetration [43]. Besides, the gel fraction values remained above 95% for all formulations, confirming efficient physical crosslinking through repeated crystallization and hydrogen bonding [44].

Under these systematically selected conditions (0.3% CS, 10.0% PVA, five freeze-thaw cycles), the swelling behavior and gel fraction of BLE-loaded hydrogels were subsequently evaluated (Fig 3(b) and

3(c)). All samples exhibited a rapid initial swelling within the first 3 h, followed by a plateau at 208–220%, suggesting equilibrium hydration of the physically crosslinked PVA/CS/BLE network. The incorporation of BLE caused a slight reduction in the equilibrium swelling ratio as BLE content increased from 0 to 4000 μg/mL. This reduction can be attributed to pore filling by BLE (Fig 2) via hydrogen bonding between phenolic groups in BLE and the polymer matrix, which decreased the effective free volume available for water uptake. Despite this modest decrease, the hydrogels retained high swelling capability, ensuring sufficient moisture retention for wound environments.

The gel fraction of BLE-loaded hydrogels decreased marginally from 95.3 ± 1.7% (blank hydrogel) to 89.6 ± 0.2% (4000 μg/mL BLE), indicating that BLE incorporation slightly interfered with the formation of crystalline PVA domains during the freeze-thaw process. The consistently high gel fraction (> 89%) demonstrates that BLE acted primarily as a physically embedded rather than disruptive component within the network. For objective evaluation, the gel fraction of the PVA/CS/BLE hydrogel is higher than that of ofloxacin-loaded PVA/CS hydrogels (80.8 ± 1.2%) developed for local anti-inflammatory treatment [45] and caffeic acid-loaded PVA/CS hybrid hydrogels (70–80%) designed for wound healing applications [46]. The combination of stable crosslinking, high water absorption, and BLE-induced compaction highlights the structural robustness of the PVA/CS/BLE system, which maintains a delicate balance between mechanical integrity and hydration responsiveness - essential for sustained bioactive release and optimal wound-healing performance. Moreover, the swelling ratio of the PVA/CS/BLE hydrogel was comparable to that of PVA/CS systems reported for similar biomedical applications, such as hydrogels encapsulating *Piper crocatum* extract (205–222%) for antibacterial use [6], and those incorporating (210–261%) for chronic diabetic wound healing [12]. Notably, PVA/CS/BLE hydrogel exhibited a substantially higher swelling capacity than PVA/CS hydrogels embedding cerium oxide nanoparticles (80–90%), designed for wound-healing applications [47]. The swelling capacity of PVA/CS/BLE hydrogel patch is also comparable to that of some commercial hydrogel dressings for the treatment of exuding wounds, such as DuoDERM® ET and Acticoat◊ (approximately 210%) [48], highlighting its effective hydrophilicity and water-retention capability suitable for wound dressing applications.

Tensile Properties of the Hybrid Hydrogels

Tensile strength, tensile modulus, and elongation at break are key mechanical parameters for evaluating the mechanical properties of a hydrogel patch in wound dressing applications. Tensile strength reflects the maximum stress the hydrogel can withstand before failure, indicating the structural integrity and cohesiveness of the polymer network, with higher values suggesting better resistance to tearing during handling or external friction [49]. Tensile modulus describes the hydrogel's stiffness and resistance to elastic deformation [50]. Elongation at break reflects the hydrogel's ductility, indicating its ability to adapt to body movements without losing structural integrity or detaching from the wound site [51].

The mechanical properties of the hybrid hydrogels were significantly affected by the incorporation of BLE (Table 1, Fig 3(d)). The pristine PVA/CS hydrogel demonstrated a tensile modulus of 92.80 kPa, a tensile strength of 549.58 kPa, and a strain at break of 150.49%,

Table 1. Tensile properties of hybrid hydrogels with increasing BLE content

CS content (%)	PVA content (%)	BLE content (μg/mL)	Tensile modulus (kPa)	Tensile strength (kPa)	Strain at break (%)
0.30	10.00	0	92.80	549.58	150.49
0.30	10.00	2000	106.60	448.00	172.94
0.30	10.00	3000	122.00	672.00	242.89
0.30	10.00	4000	81.10	296.27	141.02

indicating a flexible structure that is physically crosslinked through hydrogen bonding between PVA and CS. With the addition of BLE, both the tensile modulus and elongation at break initially increased, reaching maximum values of 122.00 kPa and 242.89% at a BLE content of 3000 μg/mL, respectively. This improvement is attributed to the strong intermolecular interactions between BLE and the polymer matrix, which reinforced the network through secondary hydrogen bonding. The simultaneous increase in strength and flexibility indicates that BLE served as a dual-function additive, both plasticizing and reinforcing, which optimized interchain compatibility and energy dissipation during deformation.

At a higher BLE concentration (4000 μg/mL), the mechanical properties were significantly compromised, with a tensile strength of 296.27 kPa and a strain at break of 141.02%. The excessive amount of BLE likely disrupted the uniformity of the polymer network and weakened the intermolecular cohesion, leading to phase separation and a decrease in the effective crosslinking density [52-53]. This trend is consistent with the morphological observations, which indicated that the excessive BLE obstructed polymer entanglement. The formulation containing 3000 μg/mL BLE exhibited the highest tensile strength (672.00 kPa), elastic modulus (122.00 kPa), and elongation at break (242.89%). These characteristics reflect a strong yet compliant network that can conform to irregular wound surfaces. Compared with previous PVA/CS-based dressings, the present hydrogel demonstrates markedly enhanced or comparable mechanical performance. For example, the tensile strength of PVA/CS/BLE hydrogel is about 73-fold higher than that of PVA/CS/gallic acid hydrogels (9.22 kPa), while its elongation at break is also significantly greater (nearly 1.5-fold) [14]. In comparison with PVA/CS/nano zinc oxide hydrogels, the tensile strength of PVA/CS/BLE hydrogel is slightly higher, while the elongation at break is comparable (242.89 vs. 250.00%), although the elastic modulus is much lower (122.00 vs. 250.00 kPa), indicating a more compliant yet mechanically robust network suitable for wound adaptation [54]. In addition, the elastic modulus of PVA/CS/BLE hydrogel is comparable to that of several commercial hydrogel dressings, such as Mepilex®, Hydrosorb®, and DuoDERM® ET [48], indicating that the PVA/CS/BLE hydrogel possesses appropriate mechanical stiffness and flexibility to maintain structural integrity, thereby supporting effective exudate management.

In this context, BLE acts as a multifunctional additive due to its phenolic and hydroxyl groups, which enhance hydrogen bonding and interchain cohesion while providing plasticizing effects. This dual effect accounts for the improved balance between tensile strength and flexibility observed. Such mechanical behavior is particularly beneficial for hydrogel patches, which require both structural integrity and conformability during wound application.

In Vitro Release Profile of PVA/CS/BLE Hydrogel

The cumulative BLE release profiles from the PVA/CS/BLE hydrogels are presented in Fig 4. All specimens exhibited a typical biphasic release pattern, characterized by an initial burst phase within the first hour followed by a slower, sustained diffusion stage. The rapid release at the early stage could be attributed to the diffusion of surface-associated BLE molecules and the high hydration rate of the hydrogel network. Increasing BLE loading from 2000 to 4000 μg/mL slightly declined the CDR (Fig 4(a,b)), likely due to stronger polymer-drug interactions at higher BLE levels. After 24 h, the CDR reached approximately 50–69%, indicating effective yet controlled diffusion through the polymer matrix.

The pH-responsive behavior of the PVA/CS/BLE hydrogels is clearly evidenced in Fig 4(c,d). At the mildly acidic condition (pH 6.5), mimicking acute inflamed tissue, the hydrogels exhibited a markedly higher release rate than at physiological pH 7.4. This difference arises from protonation of the amino groups on CS under acidic conditions, leading to enhanced electrostatic repulsion and network expansion, which in turn facilitates faster BLE diffusion. Conversely, at pH 7.4, deprotonation of the CS chains results in a more compact structure and reduced swelling, retarding BLE release. Such pH-sensitive release demonstrates the ability of the hybrid hydrogel to respond selectively to the wound microenvironment. The promoted BLE release under mild acidic conditions is therapeutically advantageous.

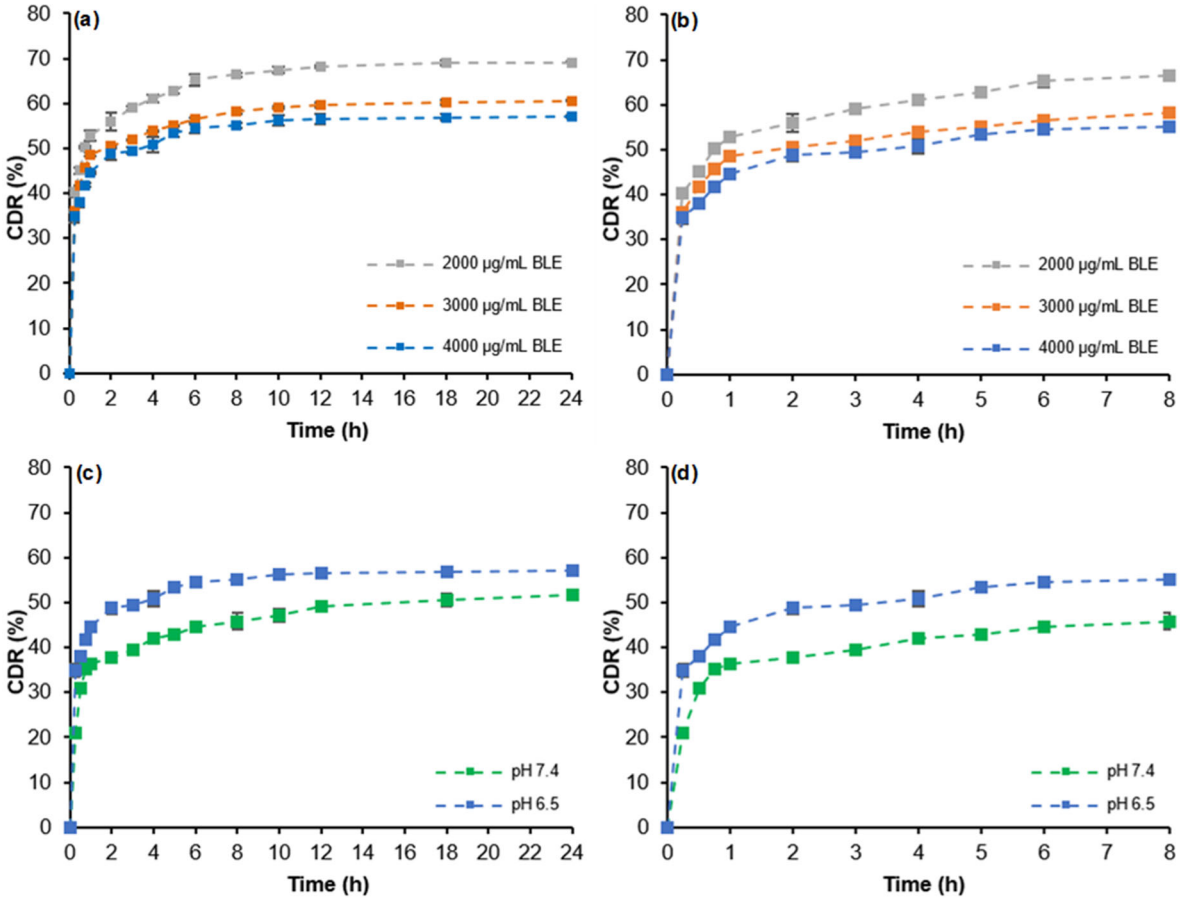

Fig 4. (a,b) Effect of BLE loading on release kinetics of PVA/CS/BLE hydrogels, (c,d) pH-responsive release profile of PVA/CS/BLE hydrogel containing 4000 µg/mL. Data are shown (a,c) over 24 h and (b,d) during the initial 8 h

Table 2. Analysis of BLE release kinetics using the Weibull model

Parameter	pH 6.5			pH 7.4
	2000 µg/mL BLE	3000 µg/mL BLE	4000 µg/mL BLE	4000 µg/mL BLE
A	0.384	0.356	0.389	0.867
B	0.348	0.373	0.413	0.388
R^2	0.970	0.968	0.972	0.945

During the early stage of acute inflammation, the wound milieu typically exhibits pH values around 6.5, where rapid BLE release can deliver bioactive compounds to exert immediate anti-inflammatory, antioxidant, and antibacterial effects. As the local pH gradually returns toward neutral during healing [55]. The slower diffusion at pH 7.4 helps sustain BLE availability, maintaining redox balance and preventing microbial regrowth. This dual-phase, pH-responsive behavior highlights the potential of PVA/CS/BLE hydrogels as intelligent wound patches capable of providing burst release for early inflammation control, followed by prolonged protection during tissue repair.

The BLE release profiles from hydrogel patches were analyzed using the Weibull model, and the fitting parameters are summarized in Table 2. The high correlation coefficients (R^2) in the range of 0.945–0.972 indicate that the Weibull equation adequately describes the release behavior across all formulations and pH conditions. The scale parameter (A) reflects the time dependence of the release process, where a lower A value corresponds to a faster release rate. At pH 6.5, the A

value ranged from 0.356 to 0.389, showing comparable diffusion rates among hydrogels with different BLE loadings. However, the A value increased markedly to 0.867 at pH 7.4, suggesting a slower, more sustained release under neutral conditions, likely due to reduced swelling of the hydrogel network at higher pH.

The shape parameter (B) provides insight into the release mechanism. In all samples, B values were below 0.45, indicating that BLE diffusion was predominantly governed by Fickian transport through the hydrogel matrix. The slightly higher B values at increased BLE concentration imply a modest transition toward anomalous diffusion, which may arise from localized interactions between BLE molecules and polymer functional groups that hinder uniform diffusion. Overall, these results confirm that BLE release from the PVA/CS hydrogel is diffusion-controlled, with the release rate modulated by both BLE loading and pH-dependent swelling behavior.

In summary, the freeze-thawed PVA/CS/BLE hydrogel serves as a "smart" hydrogel patch, effectively addressing the intrinsic therapeutic limitations of BLE when applied topically to the wound site. This bio-platform leverages the pH-sensitivity of CS to modulate the delivery of BLE in direct response to the wound microenvironment. Specifically, the hydrogel provides a critical "burst" release under mildly acidic conditions (pH 6.5) typical of acute infection and inflammation to rapidly exert antibacterial effects, reduce oxidative stress, and suppress inflammatory responses during the early stage of wound healing, followed by a sustained release profile to support prolonged therapeutic action. By successfully integrating the multiple bioactivities of BLE into a physically crosslinked, responsive network, this system bridges the gap between traditional herbal medicine and "smart" biomaterials, offering a robust and biocompatible platform for advanced wound-healing applications.

■ CONCLUSION

This study introduced a novel freeze-thawed PVA/CS hydrogel that successfully encapsulated BLE, serving as an advanced wound dressing for topical wound healing applications. By fine-tuning the concentrations of CS and PVA, along with the freeze-thaw cycles, the hydrogel achieved a compact and cohesive internal structure. It demonstrated a high gel fraction (89.6–94.0%), excellent swelling capacity (208–220%), and enhanced tensile properties, including a tensile modulus of 122.00 kPa, a tensile strength of 672.00 kPa, and an elongation at break of 242.89%. The incorporation of BLE resulted in a transformation of the porous hydrogel into a denser structure, which contributed to a controlled, pH-responsive release profile best described by the Weibull model. Unlike previous PVA/CS-based delivery systems, this study uniquely utilized a green, crosslinker-free freeze-thaw method to produce a structurally stable, pH-responsive BLE-loaded hybrid hydrogel with improved mechanical strength due to its dual-network structure. Future research may focus on *in vivo* wound healing studies and scaling up manufacturing processes. Overall, the BLE-loaded freeze-thawed PVA/CS hydrogel presents a promising platform for advanced, nature-inspired wound care solutions.

■ ACKNOWLEDGMENTS

This research is funded by Vietnam National University Ho Chi Minh City (VNU-HCM) under grant number: B2024-20-28. We acknowledge Ho Chi Minh City University of Technology (HCMUT), VNU-HCM and Institute for Tropical Technology (VITTEP) for supporting this study.

■ CONFLICT OF INTEREST

The authors have no relevant financial or non-financial interests to disclose.

■ AUTHOR CONTRIBUTIONS

Nga Hoang Nguyen Do performed the investigation and formal analysis, contributed to visualization, wrote the original draft, and reviewed and edited the manuscript; Ha Vu Le and Khoa Dang Nguyen contributed to the methodology, and reviewed and edited the manuscript; Anh Cam Ha contributed to the conceptualization, supervised the project, acquired funding, and reviewed and edited the manuscript. All authors agreed to the final version of this manuscript.

■ REFERENCES

[1] Do, N.H.N., Le, H.V., Nguyen, K.D., and Ha, A.C., 2025, Prolonged release of anti-inflammatory diclofenac sodium from *in situ* loaded thermosensitive chitosan hydrogels for localized applications, *Indones. J. Chem.*, 25 (5), 1626–1636.

[2] Gherman, S.P., Biliuță, G., Bele, A., Ipate, A.M., Baron, R.I., Ochiuz, L., Șpac, A.F., and Zavastin, D.E., 2023, Biomaterials based on chitosan and polyvinyl alcohol as a drug delivery system with wound-healing effects, *Gels*, 9 (2), 122.

[3] Ning, X., Huang, J., A, Y., Yuan, N., Chen, C., and Lin, D., 2022, Research advances in mechanical properties and applications of dual network hydrogels, *Int. J. Mol. Sci.*, 23 (24), 15757.

[4] Sadek, S.A., Fahmy, S.R., Ali, S.B., Abdelfattah, M.A., Fahmy, A.M., Mansour, K.R., Abdullah, H., Mohamed, Y., Hazem, N., Fayez, A.E., Nasr, C.F., Desouky, G.K., Hassan, A.W., and Gaafar, K.M., 2025, Developing a chitosan/polyvinyl alcohol hydrogel for gastro-retentive release of ranitidine and enhanced anti-ulcerative properties, *BMC Biotechnol.*, 25 (1), 101.

[5] Figueroa-Pizano, M.D., Vélaz, I., and Martínez-Barbosa, M.E., 2020, A freeze-thawing method to prepare chitosan-poly(vinyl alcohol) hydrogels without crosslinking agents and diflunisal release studies, *J. Visualized Exp.*, 155, e59636.

[6] Edikresnha, D., Suciati, T., Suprijadi, S., and Khairurrijal, K., 2021, Freeze-thawed hydrogel loaded by *Piper crocatum* extract with *in-vitro* antibacterial and release tests, *J. Mater. Res. Technol.*, 15, 17–36.

[7] Nguyen, T.D., Nguyen, T.T., Ly, K.L., Tran, A.H., Nguyen, T.T.N., Vo, M.T., Ho, H.M., Dang, N.T.N., Vo, V.T., Nguyen, D.H., Nguyen, T.T.H., and Nguyen, T.H., 2019, *In vivo* study of the antibacterial chitosan/polyvinyl alcohol loaded with silver nanoparticle hydrogel for wound healing applications, *Int. J. Polym. Sci.*, 2019 (1), 7382717.

[8] Chopra, H., Bibi, S., Kumar, S., Khan, M.S., Kumar, P., and Singh, I., 2022, Preparation and evaluation of chitosan/PVA based hydrogel films loaded with honey for wound healing application, *Gels*, 8 (2), 111.

[9] Do, N.H.N., Truong, Q.T., Le, P.K., and Ha, A.C., 2022, Recent developments in chitosan hydrogels carrying natural bioactive compounds, *Carbohydr. Polym.*, 294, 119726.

[10] Assauqi, N.F., Lusiana, R.A., and Masruchin, N., 2025, Optimization of chitosan-PEG/ZnO hydrogel formulation with pomegranate peel extract as an alternative for wound healing, *Indones. J. Chem.*, 25 (3), 905–918.

[11] Do, N.H.N., Le, H.V., Nguyen, K.D., and Ha, A.C., 2025, Novel thermosensitive chitosan/polyvinyl alcohol composite hydrogels delivering betel leaf extract: Physicochemical characterization and release studies for localized anti-inflammatory applications, *Polym. Bull.*, 82 (12), 6525–6547.

[12] Wang, Z., Gao, S., Zhang, W., Gong, H., Xu, K., Luo, C., Zhi, W., Chen, X., Li, J., and Weng, J., 2021, Polyvinyl alcohol/chitosan composite hydrogels with sustained release of traditional Tibetan medicine for promoting chronic diabetic wound healing, *Biomater. Sci.*, 9 (10), 3821–3829.

[13] Guo, H., Luo, H., Ou, J., Zheng, J., Huang, C., Liu, F., and Ou, S., 2025, Preparation of a chitosan/polyvinyl alcohol-based dual-network hydrogel for use as a potential wound-healing material for the sustainable release of drugs, *Carbohydr. Polym.*, 348, 122822.

[14] Cui, L., Zhao, J., Wang, Y., Han, X., Kong, L., and Liang, F., 2024, Multifunctional polyvinyl alcohol/gallic acid functionalized chitosan hydrogels prepared by freeze-thaw method for potential application as wound dressings, *React. Funct. Polym.*, 197, 105866.

[15] Viswanathan, A., Sajith, S., Harini, M., Mathiyazhagan, S., and Vimal, S., 2025, Development of a *Calophyllum inophyllum*-loaded biodegradable chitosan-PVA hydrogel: A multifunctional platform for HT-29 colon cancer cell, and antidiabetic applications, *Asian Pac. J. Cancer Biol.*, 10 (4), 845–852.

[16] Liu, Y., Wang, A., Su, C., Zhu, G., Yi, F., and Xue, Z., 2024, Preparation and evaluation of chitosan/MCM-41-based spongy hydrogels loaded with tea tree oil,

Colloids Surf., A, 691, 133862.

[17] Tran, V.T., Nguyen, T.B., Nguyen, H.C., Do, N.H.N., and Le, P.K., 2023, Recent applications of natural bioactive compounds from *Piper betle* (L.) leaves in food preservation, *Food Control*, 154, 110026.

[18] Do, N.H.N., Huynh, D.M.T., Le, T.T.H., Le, T.V.N., Vuong, H.D., Nguyen, T.P.T., Quach, T.H.N., Le, P.K., and Ha, A.C., 2024, Encapsulation of anti-bacterial *Piper betle* leaf extract in thermo-sensitive and biodegradable chitosan hydrogels: Synthesis, characterization and release kinetics, *J. Porous Mater.*, 31 (6), 2291–2306.

[19] Do, N.H.N., Tran, V.T., Cao, H.M., Nguyen, H.C., Le, K.A., and Le, P.K., 2026, Novel *Piper betle* (L.) leaf extract-encapsulated chitosan nanoparticles as bioactive coatings for strawberry preservation, *J. Food Sci. Technol.*, 63 (3), 451–461

[20] Chamidah, N.L.F., Rahanti, A.B., Kadasih, M.D., Sharfina, F.D., and Rohmawati, L., 2021, Effect of adding of green betel leaf extract and honey on mechanical properties of chitosan/PVA hydrogel wound plaster, *J. Phys.: Conf. Ser.*, 2110 (1), 012013.

[21] Nha, T.T., Tuyen, D.M.K., Phu, T.H.T., and Tram, N.X.T., 2025, Polyvinyl alcohol/chitosan/gelatin hydrogel incorporated with betel leaves for enhanced wound care management, *VNUHCM J. Eng. Technol.*, 8 (2), 2548–2557.

[22] Bahta, T., Karim, A., Periasamy, G., Gebremedhin, G., ur-Rehman, N., Bitew, H., and Hagazi, K., 2020, Analgesic, anti-inflammatory and *in-vitro* hyaluronidase inhibitory properties of the leaf extract and solvent fractions of *Otostegia fruticosa* (Forssk.) Schweinf. ex Penzig, *Iran. J. Pharm. Res.*, 19 (1), 218–230.

[23] Aayush, K., Sharma, K., Singh, G.P., Chiu, I., Chavan, P., Shandilya, M., Roy, S., Ye, H., Sharma, S., and Yang, T., 2024, Development and characterization of edible and active coating based on xanthan gum nanoemulsion incorporating betel leaf extract for fresh produce preservation, *Int. J. Biol. Macromol.*, 270, 132220.

[24] Ngamsurach, P., and Praipipat, P., 2022, Antibacterial activities against *Staphylococcus aureus* and *Escherichia coli* of extracted *Piper betle* leaf materials by disc diffusion assay and batch experiments, *RSC Adv.*, 12 (40), 26435–26454.

[25] Pramanik, T., Mazumder, M.A.R., Jany, J.F., Akash, S.I., Rahman, A., and Bhuiyan, M.K.H., 2025, Functional yogurt: An approach to fortify yogurt by polyphenols extracted from Bengal currant, *Appl. Food Res.*, 5 (1), 100715.

[26] Mazumder, M.A., Tolaema, A., Chaikhemarat, P., and Rawdkuen, S., 2023, Antioxidant and anti-cytotoxicity effect of phenolic extracts from *Psidium guajava* Linn. leaves by novel assisted extraction techniques, *Foods*, 12 (12), 2336.

[27] Abdel-Aleem, E.R., Attia, E.Z., Farag, F.F., Samy, M.N., and Desoukey, S.Y., 2019, Total phenolic and flavonoid contents and antioxidant, anti-inflammatory, analgesic, antipyretic and antidiabetic activities of *Cordia myxa* L. leaves, *Clin. Phytosci.*, 5 (1), 29.

[28] Akinwunmi, K., Odunsi, E., Amadi, C., and Ajayi, E., 2021, Anti-inflammatory and antibacterial potentials of the leaf extract and fractions of *Chrysanthemum procumetens*, *J. Herbs, Spices Med. Plants*, 27 (3), 242–252.

[29] Kaundal, R., Kumar, R., and Kumar, D., 2025, Optimized extraction technique and solvent to enhance the recovery of bioactive polyphenols from *Viola canescens* wall. Ex Roxb. A case study using OFAT and chemical characterization using UPLC-PDA, UHPLC-Q-TOF-IMS and GC–MS, *Microchem. J.*, 212, 113170.

[30] Lu, J., Zhao, Z., Pan, L., Wu, H., Wang, S., Tong, X., and Wu, S., 2025, Hyaluronidase: Structure, mechanism of action, diseases and therapeutic targets, *Mol. Biomed.*, 6 (1), 50.

[31] Pin, K.Y., Chuah, A.L., Rashih, A.A., Mazura, M.P., Fadzureena, J., Vimala, S., and Rasadah, M.A., 2010, Antioxidant and anti-inflammatory activities of extracts of betel leaves (*Piper betle*) from solvents with different polarities, *J. Trop. For. Sci.*, 22 (4), 448–455.

[32] Lugrin, J., Rosenblatt-Velin, N., Parapanov, R., and Liaudet, L., 2014, The role of oxidative stress during

inflammatory processes, *Biol. Chem.*, 395 (2), 203–230.

[33] Madhumita, M., Guha, P., and Nag, A., 2020, Bio-actives of betel leaf (*Piper betle* L.): A comprehensive review on extraction, isolation, characterization, and biological activity, *Phytother. Res.*, 34 (10), 2609–2627.

[34] Nayaka, N.M.D.M.W., Sasadara, M.M.V., Sanjaya, D.A., Yuda, P.E.S.K., Dewi, N.L.K.A.A., Cahyaningsih, E., and Hartati, R., 2021, *Piper betle* (L): Recent review of antibacterial and antifungal properties, safety profiles, and commercial applications, *Molecules*, 26 (8), 2321.

[35] Górniak, I., Bartoszewski, R., and Króliczewski, J., 2019, Comprehensive review of antimicrobial activities of plant flavonoids, *Phytochem. Rev.*, 18 (1), 241–272.

[36] Yadav, M.K., Chae, S.W., Im, G.J., Chung, J.W., and Song, J.J., 2015, Eugenol: A phyto-compound effective against methicillin-resistant and methicillin-sensitive *Staphylococcus aureus* clinical strain biofilms, *PLoS One*, 10 (3), e0119564.

[37] Buru, A.S., Neela, V.K., Mohandas, K., and Pichika, M.R., 2022, Microarray analysis of the genomic effect of eugenol on methicillin-resistant *Staphylococcus aureus*, *Molecules*, 27 (10), 3249.

[38] Hussain, R.M., Abdullah, N.F., and Amom, Z., 2016, Killing of *Staphylococcus aureus* by allylpyrocatechol is potentiated by induction of intracellular oxidative stress and inhibition of catalase activity, *J. Integr. Med.*, 14 (6), 456–464.

[39] Koosha, M., Aalipour, H., Sarraf Shirazi, M.J., Jebali, A., Chi, H., Hamedi, S., Wang, N., Li, T., and Moravvej, H., 2021, Physically crosslinked chitosan/PVA hydrogels containing honey and allantoin with long-term biocompatibility for skin wound repair: An *in vitro* and *in vivo* study, *J. Funct. Biomater.*, 12 (4), 61.

[40] Feng, X., Hou, X., Cui, C., Sun, S., Sadik, S., Wu, S., and Zhou, F., 2021, Mechanical and antibacterial properties of tannic acid-encapsulated carboxymethyl chitosan/polyvinyl alcohol hydrogels, *Eng. Regener.*, 2, 57–62.

[41] Thanh, N.Q., Mai, D.H., Le, T.P.A., Do, N.H.N., and Le, P.K., 2025, Novel chitosan/polyvinyl alcohol gel encapsulating ethanolic *Centella asiatica* extract for cosmeceutical applications, *Polym. Bull.*, 82 (2), 523–541.

[42] Chang, L., Kong, B., Liu, Q., Du, X., and Xia, X., 2025, Effect of freeze-thaw processes on the water-absorption ability and mechanical properties of hydrogel pads with chitosan/poly(vinyl alcohol) based on citrate crosslinks, *Food Chem.*, 471, 142785.

[43] Gupta, S., Goswami, S., and Sinha, A., 2012, A combined effect of freeze-thaw cycles and polymer concentration on the structure and mechanical properties of transparent PVA gels, *Biomed. Mater.*, 7 (1), 015006.

[44] Chen, Y., Chen, J., Chen, K., and Qiu, H., 2024, Preparation and properties of antibacterial composite hydrogels based on polyvinyl alcohol, chitosan, and nano-metal oxide, *Cellulose*, 31 (6), 3607–3622.

[45] Kumari, P., Shukla, M.K., Tripathi, A., Pandey, J., and Goyal, A.K., 2025, Development of ofloxacin-loaded CS/PVA hydrogel for the treatment of metritis in bovine, *Drugs Drug Candidates*, 4 (2), 17.

[46] Kenawy, E.R., Kamoun, E.A., Elsigeny, S.M., Heikal, S., El-Shehawy, A.A., and Mahmoud, Y.A.G., 2026, Caffeic acid loaded-physically crosslinked PVA/chitosan hybrid hydrogel membranes for local wound healing: Synthesis and *in vitro* assessments, *J. Polym. Res.*, 33 (2), 37.

[47] Kalantari, K., Mostafavi, E., Saleh, B., Soltantabar, P., and Webster, T.J., 2020, Chitosan/PVA hydrogels incorporated with green synthesized cerium oxide nanoparticles for wound healing applications, *Eur. Polym. J.*, 134, 109853.

[48] Minsart, M., Van Vlierberghe, S., Dubruel, P., and Mignon, A., 2022, Commercial wound dressings for the treatment of exuding wounds: An in-depth physico-chemical comparative study, *Burns Trauma*, 10, tkac024.

[49] Demeter, M., Scărişoreanu, A., and Călina, I., 2023, State of the art of hydrogel wound dressings developed by ionizing radiation, *Gels*, 9 (1), 55.

[50] Aderibigbe, B.A., 2022, Hybrid-based wound dressings: Combination of synthetic and biopolymers, *Polymers*, 14 (18), 3806.

[51] Yu, P., Wei, L., Yang, Z., Liu, X., Ma, H., Zhao, J., Liu, L., Wang, L., Chen, R., and Cheng, Y., 2024, Hydrogel wound dressings accelerating healing process of wounds in movable parts, *Int. J. Mol. Sci.*, 25 (12), 6610.

[52] Shamloo, A., Aghababaie, Z., Afjoul, H., Jami, M., Bidgoli, M.R., Vossoughi, M., Ramazani, A., and Kamyabhesari, K., 2021, Fabrication and evaluation of chitosan/gelatin/PVA hydrogel incorporating honey for wound healing applications: An *in vitro*, *in vivo* study, *Int. J. Pharm.*, 592, 120068.

[53] Waresindo, W.X., Luthfianti, H.R., Edikresnha, D., Suciati, T., Noor, F.A., and Khairurrijal, K., 2021, A freeze–thaw PVA hydrogel loaded with guava leaf extract: Physical and antibacterial properties, *RSC Adv.*, 11 (48), 30156–30171.

[54] Khorasani, M.T., Joorabloo, A., Adeli, H., Mansoori-Moghadam, Z., and Moghaddam, A., 2019, Design and optimization of process parameters of polyvinyl (alcohol)/chitosan/nano zinc oxide hydrogels as wound healing materials, *Carbohydr. Polym.*, 207, 542–554.

[55] Das, I.J., and Bal, T., 2024, pH factors in chronic wound and pH-responsive polysaccharide-based hydrogel dressings, *Int. J. Biol. Macromol.*, 279, 135118.